EXPERIMENTAL STUDY ON THE PERFORMANCE OF AN AIR-SOURCE MULTI-FUNCTIONAL HEAT PUMP FOR COMMERCIAL BUILDINGS

by

Fuqiang QIU[a*], Peng LI[a], Han XU[a], Jie LI[a], Xingwei ZHANG[b]

[a]School of Electrical Engineering, Tongling University, Tongling, China
[b]Xinxiang Chemical Fiber Co., Ltd, Xinxiang, China.

Original scientific paper
https://doi.org/10.2298/TSCI2602005Q

This paper presents a novel air-source multi-functional heat pump (AMHP) for commercial buildings. The AMHP integrates refrigeration, space heating, water heating, and heat recovery functions into a single device, offering a comprehensive solution for commercial building heating and cooling needs. The objective is twofold: to enhance energy efficiency and to reduce environmental impact. A series of experiments were conducted to assess its performance across a range of operating modes and ambient conditions. The findings indicate that the AMHP can function reliably over an extended period, thereby achieving substantial energy savings. This research provides a pragmatic and energy-efficient solution for a range of applications in commercial buildings. Further system design optimization is proposed for subsequent studies.

Keywords: *air-source heat pump, multi-functional, refrigeration, space heating, water heating, heat recovery, energy efficiency*

Introduction

In the contemporary period of accelerated global urbanization and industrialization, there has been a dramatic increase in the energy demands of commercial buildings [1, 2]. This escalating consumption has been shown to drive up operational costs significantly and exacerbate environmental challenges [3], especially in the face of climate change [4], and resource scarcity [5]. It is imperative to acknowledge the considerable share of global energy consumption that is attributed to building energy systems. This underscores the urgency of enhancing their energy efficiency, a matter that has come to the fore as a pressing concern [6]. Among these systems, HVAC systems [7] are of paramount importance, as they are typically responsible for a significant proportion of the total energy consumption of a building. Consequently, the development of sophisticated HVAC technologies capable of concurrently enhancing energy efficiency and reducing environmental impact has emerged as a pivotal research imperative.

In recent years, heat pumps have emerged as a promising solution to these challenges [8, 9]. The integration of multiple functions into a unified heat pump system has the potential to enhance energy utilization and reduce waste. For instance, the recovery of condensation heat from the cooling process for domestic hot water heating has been demonstrated to result in significant energy savings [10, 11]. This has been demonstrated to enhance the overall system efficiency and concurrently reduce the carbon footprint associated with energy consumption [12].

* Corresponding author, e-mail: 549977856@qq.com

Qiu *et al.* [13] introduced a domestic condensing heat recovery air conditioner. Chiu *et al.* [14] conducted a series of experiments on a heat recovery system with the objective of reducing the carbon footprint of smart buildings. Sun *et al.* [15] investigated the performance of four condensation heat recovery systems in full and partial condensing heat recovery modes. Roomi and Theeb [16] conceived a finned helical coil heat exchanger, with the objective of enhancing the performance coefficient of a waste heat recovery system. Chen *et al.* [17] developed a novel dedicated outdoor air conditioning system with double heat recovery. Chen *et al.* [18] conducted a study on energy-saving techniques for central air-conditioning cooling water systems, achieving a waste heat recovery efficiency, denoted as η_1, of 97.84% and an energy-saving rate, denoted as η_2, of 32.6%. Nonetheless, in spite of the myriad advantages of multi-functional heat pumps, their extensive implementation is impeded by technical challenges concerning system design, operational stability, and performance enhancement.

This study focuses on an AMHP tailored for commercial buildings. The AMHP combines refrigeration, space heating, water heating, and condensation heat recovery for sanitary water heating, building upon the concepts [19]. Through comprehensive experimental research, this study aims to assess the dynamic behavior and thermal performance of the AMHP under various operating modes and ambient conditions. The results are expected to offer valuable insights for the development and optimization of multi-functional heat pump systems, thereby facilitating more sustainable and efficient energy management in commercial buildings.

Experimental set-up

The structural diagram of the AMHP is depicted in fig. 1. The device is capable of operating year-round in four distinct modes, as outlined below. The system is designed for the provision of chilled water for space-cooling, hot water for space-heating, heat recovery for water heating, and sanitary water heating. It is particularly well-suited for subtropical and temperate regions, where the demand for space heating and sanitary hot water is prevalent. The operational schemes of each working mode adhere to the following principles.

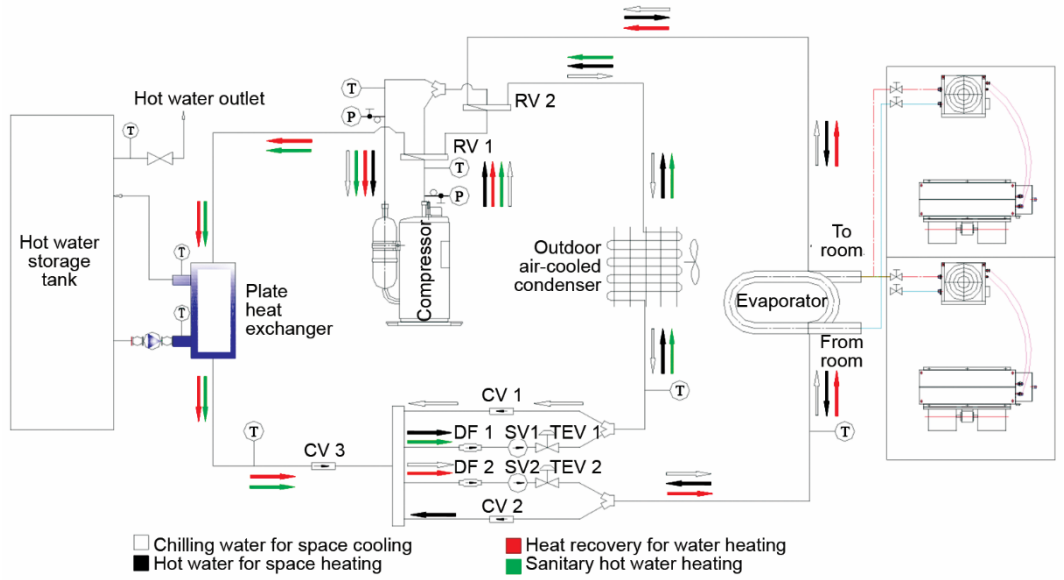

Figure 1. The elementary diagram of AMHP

The process of cooling water in space-cooling mode is a critical component of the overall system design and functionality. In circumstances where space cooling is necessary during periods of high temperature, the system functions as illustrated by the hollow arrows in fig. 1. It has been determined that the valves designated as reversing valves (FV1 and FV2) have been activated, and the solenoid valve identified as solenoid valve (SV1) is in an open position.

The utilization of hot water in space-heating mode is a crucial aspect of the system functionality. During the winter months, when space heating becomes a necessity, the FV1 and FV2 are activated, and the SV1 is opened. The direction of flow of the refrigerant is indicated by the solid arrows.

The apparatus is equipped with a mode that facilitates the heating of water in a sanitary manner. During periods of transition and winter, when the demand for sanitary hot water is at its peak, the following configuration is implemented: FV1 and FV2 are deactivated, SV1 is operational, and SV2 is in a closed state. The direction of refrigerant flow is indicated by green arrows.

The recovery of heat energy for the purpose of water heating is a process of paramount importance. During the summer months, when both space cooling and sanitary hot water are in demand, the direction of refrigerant flow is indicated by red arrows in fig. 1. The FV1 and SV2 are activated, while the FV2 and SV1 are deactivated.

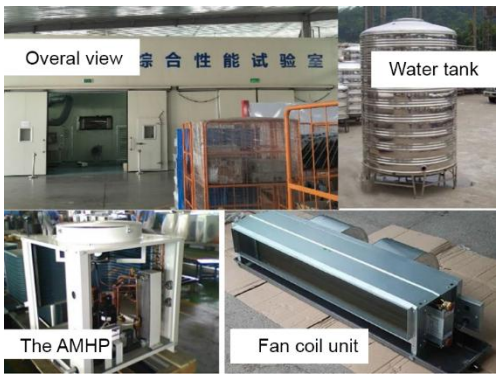

Figure 2. A figure showing the prototype of the AMHP

The prototype of the AMHP was designed and fabricated with a rated space cooling capacity of 20 kW, as illustrated in fig. 2. The primary components and the detailed parameters of each component of the system are enumerated in tab. 1. Moreover, the system incorporates a water storage tank with a capacity of 530 L.

The testing was carried out in an enthalpy laboratory (GBT7758-2010) located in Guangzhou, China. The experiment incorporated an air-handling unit to regulate the air temperature and relative humidity. As delineated in tab. 2, the testing environments are enumerated in accordance with each working mode.

A set of data acquisition systems was utilized, consisting of a Keithley data acquisition instrument, temperature sensors, thermometers, and pressure meters. The purpose of this set of instruments was to monitor, collect, and process experimental data. The testing instruments are enumerated in tab. 3:

$$Q_{\mathrm{wh}} = \rho V C_p (T_{\mathrm{w1}} - T_{\mathrm{w2}}) \tag{1}$$

where ρ is the water density (= 1000 kg/m^3), m [m^{3}h^{-1}] – the water flow rate, C_p – the specific heat capacity of water (= 4.186 kJ/kg°C), T_{w1} and T_{w2} [°C] – the initial and final water temperatures, and Δt [hours] – the time interval.

Table 1. Specifications of the main components of the AMHP

The AMHP	Quantity	
Nominal cooling capacity		20 kW
Compressor	1	Copeland: ZR72KC-TFD (scroll type, constant speed, 380 V)
Working fluid		R22
Air-cooled condenser	1	Hydrophilic film corrugated aluminum fins and inner grooved copper tubes (Axial fan rated input power: 100 W) Inner grooved copper tube (tube pitch: 25.4 mm, OD: 9.52 mm, δ:0.5 mm) Hydrophilic film corrugated aluminum fin (fin pitch:2 mm; δ:0.13 mm)
Thermostatic expansion valve	2	Emerson: BET 6
Double-pipe heat exchanger (tailored)	1	Four groups of parallel connection Inner tube: external thread copper (ID: 16.3 mm; OD: 19 mm; length: 4430 mm) Outer tube: seamless steel tube (ID: 25 mm; OD: 28 mm; length: 4680 mm) Insulation layer: black waterproof rubber thermal board (thickness:10 mm)
Plate-type heat recovery exchanger	1	DONGLIAN:EATE55 (Number of slices: 44)
Water tank	1	530 L Liner: stainless steel (ID: 480 mm; height: 1514 mm) Insulation layer: polystyrene foamed plastic

Note: OD: out diameter; ID: inner diameter

Table. 2 Testing environment of the AMHP

Testing conditions	Chilling water temperature [°C]		Outdoor ambient temperature [°C]		Mean hot water temperature in the water tank [°C]	
	T_{w1}	T_{w2}	DB	WB	T_{w1}	T_{w2}
Chilling water for space-cooling	8	12	35	24	–	–
	15	19	43		–	–
Hot water for space-heating	45	40	7	6	–	–
	45	40	2	1	–	–
Heat recovery for water heating	15	10	–	–	15	55
Sanitary hot water heating	–	–	20	14	15	55
	–	–	7	6	12	55
	–	–	2	1	12	55

Note: DB: dry bulb; WB: wet bulb

Table 3. Testing instruments

Parameters	Instrument	Model	Range	Accuracy
Air temperature and humidity	Thermometer	ROTRONIC HygroFlex	–40~85 °C	±0.1 °C ±1% RH
Water temperature	Pt100 RTD	Omega 1/10 DIN	–100~400 °C	±0.05 °C
Refrigerant temperature	Thermocouple	T-type	–400~1250 °C	±0.1 °C
Refrigerant pressure	Pressure gauge	Bourdon	–0.1~1.2 MPa –0.1~3.4 MPa	±0.3% FS
Water flow	Flow meter		0~16 m3/h	0.036 m^3/h
Power consumption	Power meter	FLUKE 39	0~10 kW	±2% FS

During testing, sanitary hot water-heating power, Q_{wh}, was calculated using:

The chilling water for space-cooling power, Q_{sc}, and hot water for space-heating power, Q_{sh}, were determined based on the water flow rate and temperature difference between the inlet and outlet of the double-pipe exchanger:

$$Q_{sc} = \dot{m}C_p(T_{w1} - T_{w2}) \tag{2}$$

$$Q_{sh} = \dot{m}C_p(T_{w1} - T_{w2}) \tag{3}$$

The coefficient of performance for sanitary water-heating, COP_{wh}, is defined:

$$COP_{wh} = \frac{Q_{wh}}{W} \tag{4}$$

where W is the input power.

The coefficient of performance for chilling water for space-cooling, COP_{sc}, is:

$$COP_{sc} = \frac{Q_{sc}}{W} \tag{5}$$

The coefficient of performance for hot water for space-heating, COP_{sh}, is:

$$COP_{sh} = \frac{Q_{sh}}{W} \tag{6}$$

The total coefficient of performance, COP_{cw}, which accounts for both Q_{sc} and Q_{wh}, is determined by:

$$COP_{cw} = \frac{Q_{sc} + Q_{wh}}{W} \tag{7}$$

Results and discussion

As illustrated in tab. 4, the testing data for the chilling water in space-cooling mode, with a water flow rate of 2.9 m^3/h, is presented. The data were collected subsequent to an additional two hours of stable system operation. In this context, W represents the combined power consumption of the compressor and fan. As illustrated in tab. 4, the suction and dis-

charge pressures, P_s/P_d, were measured at 1.69/0.45 MPa and 2.4/0.53 MPa for ambient temperatures of 35 °C and 43 °C, respectively. Consequently, the suction and discharge temperatures, T_s/T_d, were recorded as 83.6/8.7 °C and 100.9/14.2 °C, respectively. The input power values, W, were 4896 W and 6428 W, respectively. The chilling water power, Q_{sc}, was determined to be 14.72 kW and 13.46 kW, respectively. Consequently, the coefficient of performance, COP_{sc}, was calculated to be 3.01 and 2.69 under the two testing conditions.

As illustrated in tab. 5, the testing data for the space-heating mode in the cold season is presented. The recorded Q_{sh} represents the maximum value measured after a two-hours delay from the onset of stable system operation. Throughout the experiment, the defrosting process was executed five times, with each cycle lasting three minutes. The measured input power, W, is indicative of the aggregate power consumption of the compressor and fan.

During the course of the testing process, the inlet hot water temperature was maintained at 40 °C, and the water flow rate was adjusted to maintain an approximate difference of 5 °C between the inlet and outlet hot water temperatures. As demonstrated in tab. 5, the space-heating power, Q_{sh}, was measured to be 19.78 kW and 19.27 kW, respectively. The coefficient of performance for space-heating, COP_{sh}, was determined to be 3.63 and 3.61 under outdoor ambient conditions of 7 °C and 2 °C, respectively.

Table 4. The thermal performance of the AMHP in chilling water for space-cooling mode

OT [°C]	t_{w1}/t_{w2} [°C]	P_d/P_s [MPa]	T_d/t_s [°C]	W [W]	Q_{sc} [W]	COP_{sc}
35	8/12	1.69/0.45	83.6/8.7	4896	14717	3.01
43	15/19	2.4/0.53	100.9/14.2	6428	13463	2.69

Note: t_{w1} – inlet water temperature, t_{w2} – outlet water temperature

Table 5. The thermal performance of the AMHP in hot water for space-heating mode

OT [°C]	t_{w1}/t_{w2} [°C]	P_d/P_s [MPa]	T_d/t_s [°C]	W [W]	Q_{sh} [W]	COP_{sh}
7	40/45.3	1.9/0.32	97.5/1.2	5450	19780	3.63
2	40/45.5	2.01/0.27	100.5/-3.4	5337	19266	3.61

As illustrated in fig. 3, the thermodynamic performance of the AMHP in the water heating mode is demonstrated. The experiments were conducted at outdoor dry bulb temperatures of 20 °C, 7 °C, and 2 °C, respectively. The water flow rate was maintained at 4.1 m³/h. The termination of the experiments occurred when the temperature of the hot water in the storage tank reached 55 °C.

As illustrated in fig. 3(a), the discharge temperature of the AMHP increases in the sanitary hot water heating mode as time elapses, while the suction temperature remains relatively constant. The increase in discharge temperature is attributable to the rise in pressure ratio, which leads to a decrease in the flow of refrigerant through the compressor. This, in turn, results in inadequate cooling of the compressor. The constant suction temperature is primarily attributable to the active regulation of the thermal expansion valve, which effectively maintains a consistent refrigerant flow into the evaporator.

Throughout the experiment, as the outdoor ambient temperature decreased, the suction temperature of the system underwent a notable decline, attributable to the reduction in evaporation temperature. Concurrently, the discharge temperature exhibited an increase,

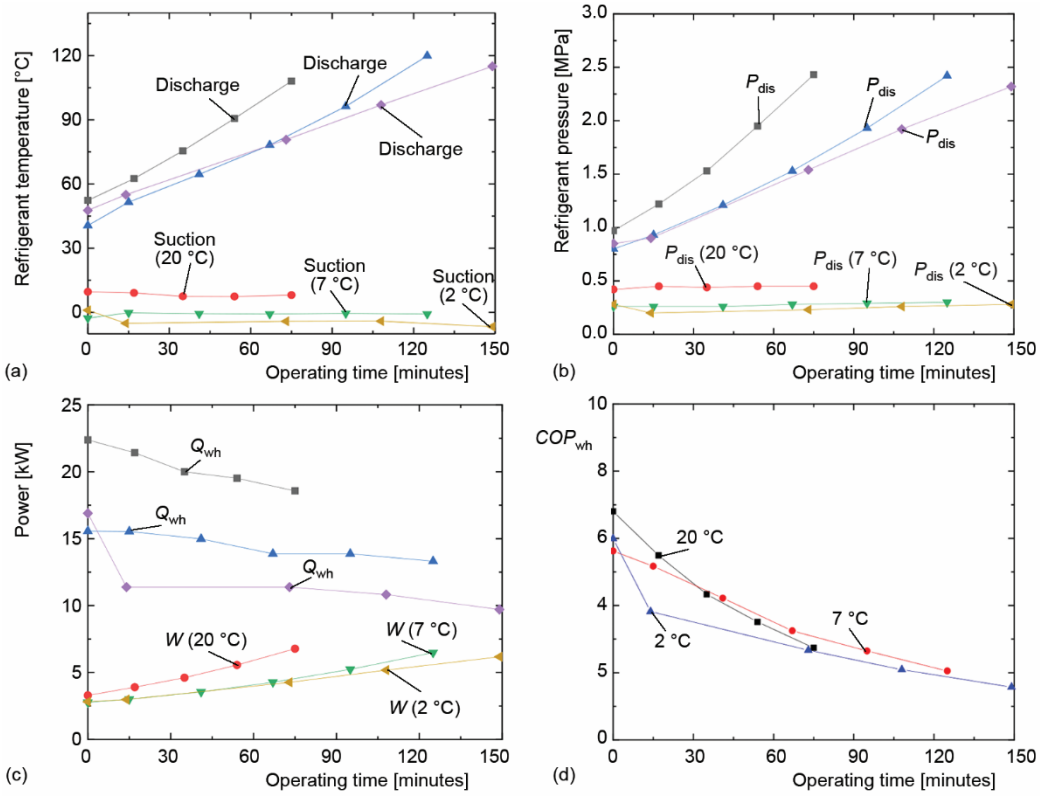

Figure 3. Variations of (a) refrigerant temperature, (b) refrigerant pressure, (c) power, and (d) COP of the AMHP in water heating mode

which can be ascribed to the diminution of refrigerant flow through the compressor, consequent to the rise in pressure ratio. In order to extend the service life of the compressor, it is essential to maintain an optimal temperature setting for the hot water supply. It is also inadvisable to operate the compressor at an ambient temperature that is excessively low.

As illustrated in fig. 3(b), the variations in refrigerant pressure of the AMHP demonstrate a persistent upward trend in discharge pressure, accompanied by negligible fluctuations in suction pressure as operating time progresses. Consequently, the compression ratio also increases. The increase in pressure ratio will decrease the gas transmission coefficient of the compressor, thereby reducing the refrigerant mass-flow through the compressor. The observed rise in discharge pressure is attributable to the concurrent rise in hot water on the condensation side, resulting in an increase in condensation pressure. However, the unobvious change of suction pressure over time can be attributed to the active regulation of the thermal expansion valve, which is designed to maintain the superheat at a constant value at a specific ambient temperature.

As ambient temperature increases, the suction pressure of the AMHP increases significantly, while the discharge pressure undergoes only slight changes. Consequently, the compression ratio undergoes a decline. The observed rise in suction pressure can be attributed to the rise in refrigerant gasification in the evaporator, which is itself caused by an increase in ambient temperature. This rise in gasification leads to an increase in evaporation pressure. In

order to maintain a constant superheat, the expansion valve is opened, thereby increasing the flow of refrigeration into the evaporator. This, in turn, results in an increase in suction pressure. The decline in pressure ratio is known to result in an augmentation of the refrigerant mass-flow through the compressor.

As illustrated in fig. 3(c), the variation in AMHP power with operating time is demonstrated under different operating conditions. The instantaneous Q_{wh} of the AMHP decreases over operating time, likely due to the reduction in refrigerant mass flux through the compressor caused by an increased pressure ratio. Despite the rise in the unit mass heat of the refrigerant in the condenser during this period, the net effect is a decrease in Q_{wh}.

The rise in instantaneous W of the AMHP over operating time can be attributed to the rise in the unit mass input power of the refrigerant through the compressor, despite the reduced mass-flow rate. As demonstrated in fig. 3, a decline in ambient temperature results in a substantial decrease in Q_{wh}, attributable to the diminished mass-flow rate of refrigerant through the compressor into the condenser. This phenomenon arises from the elevated pressure ratio. Concurrently, the average W is less influenced by the ambient temperature due to the augmented unit mass input power of the refrigerant flowing through the compressor.

The experimental findings reveal that the mean Q_{wh} of the AMHP is 19.73 kW, 13.61 kW, and 11.42 kW, respectively, while W is 4.76 kW, 4.25 kW, and 3.84 kW at ambient temperatures of 20 °C, 7 °C, and 2 °C.

As illustrated in fig. 3(d), the COP_{wh} demonstrates a persistent downward trend as the hot water temperature undergoes changes. This phenomenon can be attributed primarily to the observed decrease in Q_{wh} and the concomitant increase in W. It is noteworthy that the rate of decline in COP_{wh} exhibits a gradual flattening as the hot water temperature increases.

Additionally, the impact of ambient temperature on the COP exhibits a decline when the hot water temperature increases. As the ambient temperature is reduced, the impact of this decrease on COP_{wh} becomes less pronounced, particularly when the hot water temperature is higher.

The mean COP values were determined to be 4.14, 3.20, and 2.97 at ambient temperatures of 20 °C, 7 °C, and 2 °C, respectively.

As illustrated in fig. 4, the thermodynamic performance of the AMHP in the heat recovery for water heating mode is demonstrated. During the experiment, the inlet temperature of the chilling water was maintained at approximately 15 °C, with a constant temperature difference of 5 °C. Consequently, the mass flux of the chilling water on the evaporator side gradually decreased as the hot water temperature increased. The trend in the thermal performance of the AMHP in this mode is analogous to that observed in the sanitary hot water heating mode. In order to circumvent redundancy, the rationale underlying these modifications will not be expounded upon in this particular section.

As illustrated in fig. 4(a), the variations of refrigerant temperature in the AMHP with operating time is demonstrated. Concurrently, the discharge temperature experiences an upward trend as the hot water temperature rises. Nonetheless, the temperature of evaporation remains relatively stable due to the restricted opening of the thermal expansion valve.

As illustrated in fig. 4(b), the discharge pressure of the AMHP exhibits a continuous increase with operating time during the heat recovery for water heating mode, while the suction pressure remains relatively constant.

As illustrated in fig. 4(c), the variations of Q_{wh}, Q_{sc}, and W with operating time are demonstrated in the heat recovery for water heating mode. As operating time is increased,

both Q_{wh} and Q_{sc} demonstrate a continuous decline, while W exhibits a continuous increase. The mean values of Q_{wh} and Q_{sc} are 23.11 kW and 18.05 kW, respectively.

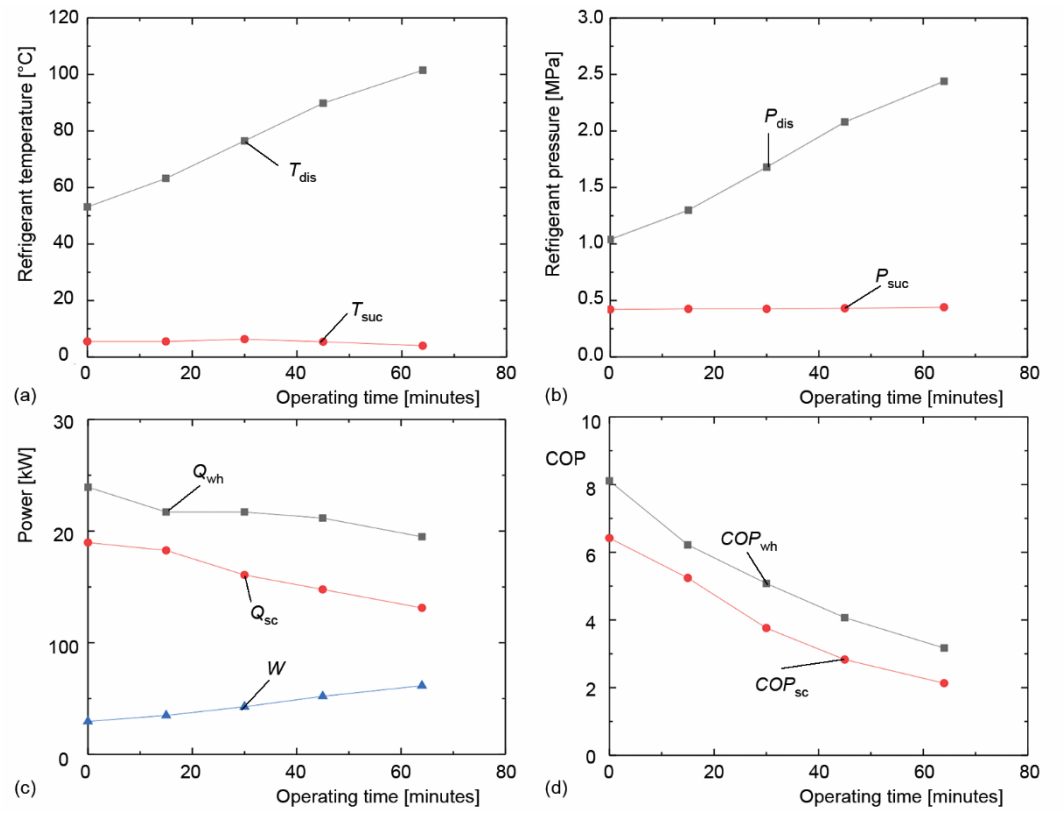

Figure 4. Variations of (a) refrigerant temperature, (b) refrigerant pressure, (c) power, and (d) COP of the AMHP in air-source mode

As illustrated in fig. 4(d), the sustained increase in Q_{sh} and Q_{sc}, concomitant with the decline in W over the operational time, leads to a continuous decrease in COP_{wh} and COP_{sc}. However, the rate of this decline gradually diminishes over time. It is noteworthy that COP_{wh} persists in exceeding COP_{sc}, with the two curves maintaining a largely parallel configuration. The computed average values of COP_{wh} and COP_{sc} for the AMHP are 4.57 and 3.57, respectively. Furthermore, the COP_{cw} attains 8.14, thereby markedly augmenting the system's comprehensive energy utilization efficiency.

Conclusions

This study experimentally evaluated the AMHP and demonstrated its stable and efficient operation across various modes. In the space-cooling mode, the AMHP achieved COP_{sc} values of 3.01 at 35 °C and 2.69 at 43 °C. For space-heating applications, the COP values were 3.63 at 7 °C and 3.61 at 2 °C. In the case of sanitary water heating, the values of COP_{wh} were determined to be 4.14 at 20 °C, 3.2 at 7 °C, and 2.97 at 2 °C. The heat recovery mode exhibited an average COP_{cw} of 8.14. The reliability of these results was confirmed by uncer-

tainty evaluations. The AMHP high efficiency and adaptability across different conditions underscore its potential for energy savings in commercial buildings. Subsequent research endeavors may concentrate on the further refinement of the system design.

Building on these results, future research will focus on optimizing the AMHP design through cross-disciplinary innovations. As proposed in [20], bio-inspired design principles offer new pathways for energy efficiency. For instance, integrating fractal geometry [21] into heat exchanger surfaces – similar to the self-similar folding patterns of clover leaves – could enhance heat transfer area while reducing material usage. Additionally, AI-driven control systems [22], informed by deep learning algorithms [23], may dynamically adjust the AMHP operation in real time, further optimizing performance under fluctuating environmental conditions.

Acknowledgment

This work was financially supported by Major Project of Anhui Provincial Department of Education for Higher Education Industry-University-Research (2025AHGXZK 60036), Horizontal Research Project of Tongling University (2025tlxyxdz179), and Key Natural Science Project of Tongling University (2025tlxykjZD10).

References

[1] Deng, Z., *et al.*, Quantification of Energy Flexibility Potential in Commercial Buildings for Demand Response across Various Climate Zones in China, *Journal of Building Engineering, 105* (2025), July, 112595
[2] Liu, Y. P., *et al.*, Clover-Inspired Fractal Architectures: Innovations in Flexible Folding Skins for Sustainable Buildings, *Fractals, 33* (2025), 2550041
[3] Xuan, V. N., Nexus of FDI, GDP, Renewable Energy, Trade Openness, and Environmental Pollution in Japan: New Evidence from ARDL Method, *Environmental and Sustainability Indicators, 26* (2025), 100677
[4] Chapagain, K., *et al.*, Impact Assessment of Climate and Land Use Change on the Water-Energy-Food Nexus: An Application to the Ping River Basin, Thailand, *Science of The Total Environment*, *971* (2025), 179067
[5] Shao, Y., *et al.*, Human Health, Ecosystem Quality, and Resource Scarcity Burdens Inflicted by Livestock Production Across Chinese Regions, *Earth's Future, 13* (2025), e2024EF005263
[6] Liu, Z., *et al.*, A Comprehensive Analysis on Definitions, Development, and Policies of Nearly Zero Energy Buildings in China, *Renewable and Sustainable Energy Reviews*, *114* (2019), 109314
[7] Garg, A., HVAC (Air-Conditioning) System, in: *Handbook on Hospital Planning & Designing*, Springer, Singapore, 2024
[8] Qiu, F. Q., *et al.*, Experimental Research on Dynamic Performance of an Air/Water Source Heat Pump Water Heater, *Thermal Science*, *28* (2024), 3A, pp. 2067-2074
[9] Bozic, J., *et al.*, Life Cycle Assessment of Energy Green Transition Goals in Slovenia and Serbia: Heat Pump Example, *Thermal Science*, *28* (2024), 6A, pp. 4709-4721
[10] Ding, Z. X., *et al.*, Solar - Driven Hygroscopic - Material - Based Absorption Thermal Battery for Global Heating Decarbonization, *Energy Storage Materials*, *77* (2025), 104184
[11] Li, W., *et al.*, Performance Analysis of Heat Recovery in CO_2 Refrigeration Systems for Heating Electrification in Supermarkets, *Applied Energy 384* (2025), 125461
[12] Sunu, P. W., *et al.*, A Brief Comparative Thermodynamics Review of Domestic Air Conditioning System with or without Installed Heat Recovery, *Journal of Physics Conference Series, 1450* (2020), 012087
[13] Qiu, F. Q., *et al.*, Experimental Investigations on the Thermal Performance of a Domestic Condensing Heat Recovery Air-Conditioner, *Advances in Mechanical Engineering 11* (2019), 1687814018822349
[14] Chiu, Y. W., *et al.*, Heat Recovery System for Reducing Smart Building Carbon Footprint, *Sensors and materials: An International Journal on Sensor Technology*, *32* (2020), 3, pp. 885-893

[15] Sun, S., *et al.*, Experimental Study on the Condensing Heat Recovery Performance of Air Source Heat Pump, *Journal of Energy Storage, 32* (2020), 101808
[16] Roomi, B. K., Theeb, M. A., Experimental and Theoretical Study of Waste Heat Recovery from a Refrigeration System Using a Finned Helical Coil Heat Exchanger, *Heat Transfer, 49* (2020), 6, pp. 3560-3574
[17] Chen,S., *et al.*, Modelica-Based Modeling and Simulation of a Novel Dedicated Outdoor Air-Conditioning System with Double Heat Recovery, *Journal of Building Engineering 99* (2025), 111535
[18] Chen, X., *et al.*, Research on Energy saving Technology of Circulating Cooling Water System in Central Air Conditioning System. *Journal of Physics: Conference Series, 2920* (2024), 012027
[19] Qiu, F. Q., *et al.*, Experimental Investigations on the Thermal Characteristics of a Multi-Functional Air-Conditioner, *International Journal of Low-Carbon Technologies*, *18* (2023), Mar., pp. 218-227
[20] Liu, Y. P, *et al.*, Clover-Inspired Fractal Architectures: Innovations in Flexible Folding Skins for Sustainable Buildings, *Fractals, 33* (2025), 2550041
[21] He, C. H., *et al.*, A Fractal-Based Approach to the Mechanical Properties of Recycled Aggregate Concretes, *Facta Universitatis, Series: Mechanical Engineering, 22* (2024), 2, pp. 329-342
[22] Cheng, Y., *et al.*, Differential Equation-Driven Intelligent Control: Integrating AI, Quantum Computing, and Adaptive Strategies for Next-Generation Industrial Automation, *Advances in Differential Equations and Control Processes, 32* (2025), 3096
[23] Karim, F. K., *et al.* Innovative Mathematical Modelling Approaches to Diagnose Chronic Neurological Disorders with Deep Learning, *Thermal Science, 28* (2024), 6B, pp. 5217-5229

Paper submitted: October 18, 2024
Paper revised: April 30, 2025
Paper accepted: May 3, 2025